Chapter 7
Examples and Material Standards

7-1. Determination of Fracture Toughness

a. General.

(1) In any linear-elastic fracture mechanics analysis, the fracture toughness, either the critical plane stress intensity factor K_{Ic} or the critical stress intensity factor K_c of the structural component must be determined. For most component geometries (thicknesses), the fracture toughness will be defined by the critical plane-stress stress intensity factor K_c. However, the critical plane-strain stress intensity factor K_{Ic} is a material property and is a lower bound for K_c.

(2) The fracture toughness (K_{Ic} or K_c) of steel increases with increasing temperature and decreasing load rate. Mild structural steels typically exhibit a relatively large increase in toughness over a certain temperature range as shown in Figure 7-1. The fracture toughness versus temperature relationship can be divided into three regions: the lower shelf region, which is characterized by relatively low toughness and small variation in toughness with temperature; the transition region, which is characterized by rapid increase of toughness with increasing temperature; and the upper shelf region, where the variation in toughness with temperature is again relatively low.

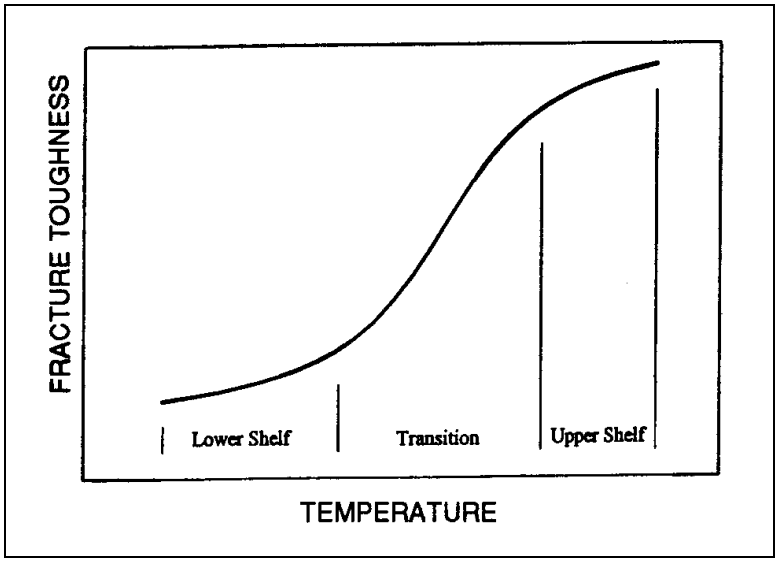

Figure 7-1. Temperature effects on fracture toughness

(3) The effect of load rate on fracture toughness is shown in Figure 7-2, which illustrates the nature of the fracture toughness versus temperature relationship for static and dynamic loading. The general shape of the temperature versus fracture toughness relationship is maintained for various loading rates. For increasing load rates, the transition region occurs at higher temperatures. (Intermediate load rate curves would lie between the static and dynamic curves shown in Figure 7-2.) For a given magnitude of fracture toughness, a temperature shift exists between fracture toughness for dynamic loading, K_{Id}, and that for slow loading rate, K_{Ic}. This empirically derived temperature shift T_s is given by Equation 7-1 (Barsom and Rolfe 1987):

$$T_s = 102 - 0.12\,\sigma_y \text{ °C, for 250 MPa} < \sigma_y < 965 \text{ MPa}$$
$$T_s = 0, \qquad \text{for } \sigma_y > 965 \text{ MPa} \tag{7-1}$$

where σ_y is the yield stress.

(For non-SI units $T_s = 215 - 1.5\ \sigma_y$ °F, for 36 ksi < σ_y < 140 ksi, and $T_s = 0$ for σ_y > 140 ksi.)

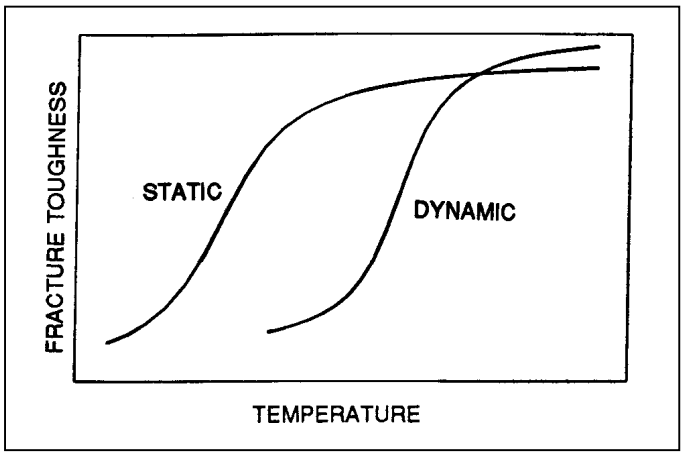

Figure 7-2. Load rate effect on toughness

b. Plane-strain fracture toughness.

(1) As described in Chapter 5, the plane-strain fracture toughness K_{Ic} is defined by ASTM E399. Unfortunately, for almost all low- to medium-strength structural steels, it is impractical if not impossible to directly determine K_{Ic} at reasonable service temperatures. One of the more common approaches to this problem has been to correlate K_{Ic} with results from other mechanical tests, most notably Charpy V-Notch (CVN). One of the commonly used correlations between CVN and K_{Ic} is the two-stage CVN-K_{Id}-K_{Ic} correlation (Barsom and Rolfe 1987). The procedure for this is as follows:

(a) Determine standard impact CVN test results in the transition temperature region. (It is desirable to test at temperatures approximately T_s above the expected minimum service temperature T_o.)

(b) Convert CVN data to K_{Id} values based on the empirical relationship

$$K_{Id} = \sqrt{0.64 \bullet \text{CVN} \bullet E} \quad \text{kPa} - \sqrt{\text{m}} \tag{7-2}$$

where

CVN = Charpy V-Notch value at the given temperature, joules
E = modulus of elasticity, kPa

(For non-SI units $K_{Id} = \sqrt{5 \bullet \text{CVN} \bullet E}$ psi $- \sqrt{\text{in.}}$, where CVN = ft-lb and E = psi.)

(c) Shift the K_{Id} values at each temperature by T_s (Equation 7-1) to determine the K_{Ic} values as a function of desired minimum service temperature: $K_{Ic}(T_o) = K_{Id}(T_o + T_s)$.

(2) The procedure for the CVN-K_{Id}-K_{Ic} correlation is illustrated in Figure 7-3. This correlation is valid only for the lower shelf region and the lower end of the transition region of the CVN curve, which limits its use for structural steels at practical service temperatures. Barsom and Rolfe (1987) have suggested that this correlation is valid for CVN values in foot-pounds that are less than one-half the yield strength in ksi.

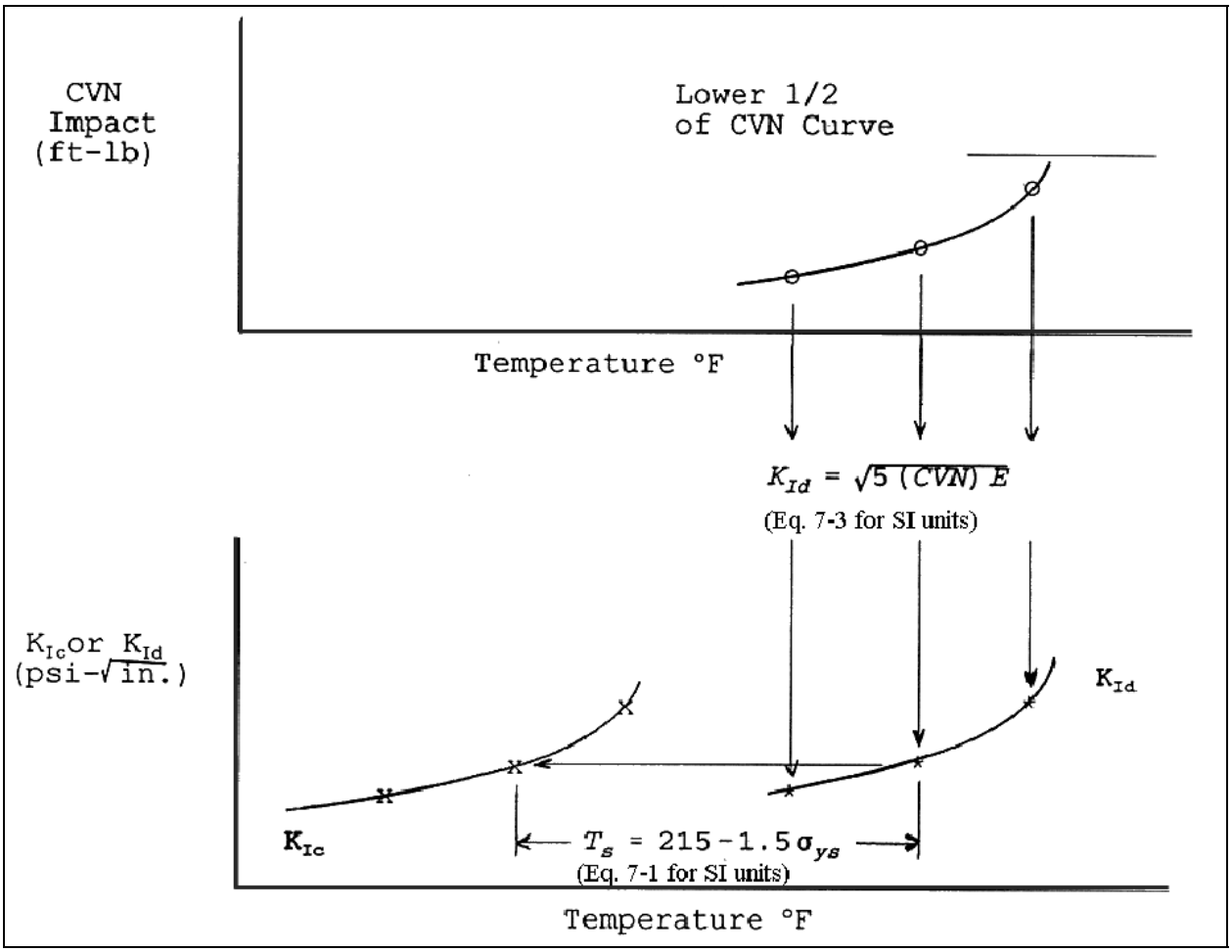

Figure 7-3. Two-stage CVN-K_{Id}-K_{Ic} correlation (°C = 5/9 (°F – 32); 1 psi-$\sqrt{in.}$ = 1.099 kPa-$\sqrt{m}$; 1 ft-lb = 1.36 J)

(3) A CVN-K_{Ic} correlation that is valid at higher temperatures in the upper shelf region is given by

$$\left(\frac{K_{Ic}}{\sigma_y}\right)^2 = 0.646\left(\frac{\text{CVN}}{\sigma_y} - 0.0098\right) \tag{7-3}$$

where

K_{Ic} = MPa - $\sqrt{\text{m}}$

σ_y = static yield stress in MPa

CVN = joules

(For non-SI units,

$$\left(\frac{K_{Ic}}{\sigma_y}\right)^2 = 5\left(\frac{\text{CVN}}{\sigma_y} - 0.05\right)$$

where K_{Ic} = ksi - $\sqrt{\text{in.}}$, σ_y = ksi, and CVN = ft-lb.)

(4) These two correlations provide estimates for the upper and lower shelf regions (Figure 7-1). K_{Ic} in the transition region can be estimated by interpolation.

c. *Plane-stress fracture toughness.* In most applications, the component or member will have insufficient thickness for plane-strain behavior. While this is generally a positive consequence since deviation from plane-strain conditions provides increasing resistance to fracture, the fracture toughness is no longer represented by K_{Ic} (except as a lower bound). The thickness required for plane-strain conditions is indicated by rearrangement of Equation 2-2:

$$t \geq 2.5 \left(\frac{K_{Ic}}{\sigma_y} \right)^2 \tag{7-4}$$

If this thickness requirement is not met, then the fracture toughness is represented by the plane-stress fracture toughness K_c, which can be estimated by various methods such as correlations with R-curve or crack tip opening displacement (CTOD) test data (Barsom and Rolfe 1987). The correlation between CTOD test data and K_c is given by

$$K_c = \sqrt{1.4\, E\, \frac{\sigma_y + \sigma_{ult}}{2}\, \delta_c} \tag{7-5}$$

where

σ_{ult} = yield and ultimate stress

δ_c = critical crack tip opening displacement as determined in accordance with ASTM E1290.

Alternatively, if the thickness is such that the plane-strain condition is nearly satisfied, K_c can be estimated by

$$K_{Ic}^2 = K_{Ic}^2 \left(1 + 1.4\, \beta_{Ic}^2 \right) \tag{7-6}$$

where β_{Ic} is given by Equation 2-2.

7-2. Example Fracture Analysis

This paragraph includes three example problems. The example in *a* below demonstrates the proposed guidelines for conducting an overall structural evaluation of a spillway gate. The example given in *c* below specifically illustrates the evaluation of a cracked member. The example in *d* below pertains to a fracture analysis on two tension members of a lock gate.

a. *Spillway gate evaluation example.* This case study is based on the results of an inspection of the riveted tainter gates at Lock and Dam 5 on the upper Mississippi River near Winona, MN. A supplemental example in *b* below is also included to illustrate a fatigue evaluation and is based on a hypothetical inspection report that indicates significant cyclic stresses have been measured in the gate. Although this example is based on a riveted spillway gate, the process illustrated is applicable to welded and riveted hydraulic steel structures.

(1) Preinspection assessment. The design documents and previous inspection reports were reviewed, critical areas were identified, and previously reported conditions noted. The tainter gates are 10.7 m (35 ft) wide, 4.57 m (15 ft) high, and 7.62 m (25 ft) in radius from the trunnion pin to the face of the skin plate. The

structure is framed similar to the standard tainter gate geometry as described by EM 1110-2-2702 with a 0.95-cm (3/8-in.) skin plate, C12 × 25 vertical ribs, two W30 × 118 horizontal girders, and W18 × 80 strut arm frames. All connections are riveted except for the use of bolts at the strut arm-trunnion block detail. The gates have Type J side seals and steel bottom seal details. The gates have a history of structural problems including significant gate vibrations and buckled web and flange plates on the strut arm. No extreme loads or unusual events had been reported since the last inspection. A change in operational practice was instituted to avoid gate opening settings that cause structural vibration. Because of the history of problems at this site, a thorough visual inspection was made previously on several gates.

(2) Inspection. An in-depth inspection was made of the gate with particular attention to the critical areas. Weather conditions at the dam site during the inspection were sunny and warm. The examination was conducted while water was being released from the gates. The following conditions were noted:

(a) Member or component deformation. Local web and flange plate buckling on the strut arms adjacent to the knee brace intersection from the upper horizontal girder was visible on several gates and is most severe on Gate 24. The condition has not deteriorated since the last inspection and was most likely caused by excessive ice loads on the structure.

(b) Seal problems. Water was observed flowing through the side seals.

(c) Rivet deterioration. Corrosion and a small amount of section loss were visible on some rivet heads.

(d) Mechanical/electrical problems. At Gate 25, one chain hoist was out of its guide on the skin plate. This hoist was toward the Minnesota side of the gate.

(e) Fabrication defects. There was no previous indication that fabrication defects existed in the structural members, and none were observed during this inspection.

(f) Corrosion. Paint loss and blistering were visible along the top surface of the web on the upper horizontal girder under the diversion plate. Blistered paint was left intact during the inspection.

(g) Fatigue cracking. No fatigue cracks were observed.

(h) Vibration or other unusual behavior. To check for vibration, the gate was fully closed and then reopened approximately 3.0 cm (0.1 ft) when vibration began. By rough measurement, the vibration frequency was estimated at 5-10 Hz. The amplitude of vibration was maximum at midspan of the gate and was sufficient to create an audible noise and make ripples in the backwater. The vibration ceased when the gate was opened further.

(i) Application of unusual loads. Except for the noted vibration, no unusual or extreme loads were reported. There was, however, an extensive accumulation of debris on the structural members in back of the skin plate, primarily large timber pieces.

(3) Evaluation. Because several detrimental conditions were detected during the inspection, the structural integrity of the spillway gate must be evaluated.

(a) Since an evaluation of the local buckling of the strut arms was conducted when it was first observed and the amount of buckling on the strut arms had not increased since the last inspection, it is believed that the structural capacity of the buckled members or of the gate is not in jeopardy at this time.

(b) The amount of water leakage from the side seals is considered tolerable and will have no effect on normal gate operations.

(c) Misalignment of the chain hoist is not severe enough to jeopardize operation of the gate but should be corrected.

(d) Deterioration due to corrosion and rivet head loss are considered minor and will have no effect on normal gate operations or gate strength.

(e) Flow-induced structural vibrations can cause serious damage to the spillway gate. In previous studies, stress ranges of approximately 27.6 MPa (4 ksi) have been calculated. Although this stress range is below the 41.4-MPa (6-ksi) threshold for fatigue crack growth at riveted details, the presence of groove welds to water-seal gaps between adjacent skin plates and tack welds to attach the diversion plate to the gate ribs may reduce this threshold stress range. However, since no fatigue cracks were detected and it is known how to control the gate vibrations, the structural capacity is not in jeopardy.

(f) Although the accumulation of debris on the gate structure has not caused any structural or corrosion problems, it should be removed.

(4) Recommendations. Based on the evaluation of conditions for the riveted tainter gates, the following recommendations are provided as steps that should be taken to ensure structural integrity for normal operations until the next regular inspection:

(a) Continue operation of the spillway gates outside the range that causes vibration.

(b) Schedule maintenance at Gate 25 to make repairs or adjustments to reinstall the chain hoist in the guide on the skin plate.

(c) Schedule maintenance to remove large debris from all gate structures.

(d) The buckled strut arm members should be occasionally monitored by lock personnel to detect any increases in deformation or distress to adjacent components.

(e) Gate vibrations should be monitored by lock personnel to detect any changes. The inspection interval should be reduced to 2 to 3 years to monitor the buckled members and any future effects of the noted vibration problem more closely.

b. Fatigue evaluation.

(1) To illustrate fatigue strength considerations, let it be assumed that during the inspection of tainter gates a more significant mode of vibration had recently been observed. Because of this new information, a thorough inspection was made at all fatigue-sensitive details on several gates where this vibration was observed. However, no fatigue cracks were visible.

(2) Based on the inspection findings in this assumed example, a field study was recommended to determine the significance of these new vibrations. The results of the field study revealed that vibrations of approximately five cycles per second or Hertz (Hz) were producing cyclic stresses of up to 55.2 MPa (8 ksi) at several details on the riveted structure.

(3) The integrity of the riveted gate structure must be assessed by determining the fatigue strength of the details that are subjected to these cyclic loads. Since the measured maximum stress range is less than

68.9 MPa (10 ksi), the Category C curve will be used to determine the approximate number of cycles to failure at the detail (this does not imply that the entire structure will fail). By projecting lines on the S_r-N curve shown in Figure 6-22, it can be determined that the number of cycles to failure is approximately 12.5 million. With the measured frequency of vibration equal to 5 Hz, it would take approximately 694 hours (29 days) of vibration at this stress range to exceed the fatigue strength of the riveted connection. But because this new mode of vibration has only recently been observed, it is probable that not many cycles have accumulated to date. In fact, unless the gates in this assumed example are allowed to vibrate for extended periods, it may take up to 3-1/2 years before fatigue cracks develop if vibrations are limited to 1/2 hour per day while the gates are being adjusted.

(4) The recommended action to address this assumed condition would consist of three steps:

- Minimize the occurrence of gate vibrations by operating outside the range causing vibration.
- Reduce the inspection interval to approximately 1 year and inspect a greater number of gates to ensure that similar vibration is not occurring.
- Begin engineering studies to determine solutions to reduce the stresses caused by these vibrations.

c. Fracture evaluation example.

(1) During an inspection, a 9-cm (3.5-in.) crack was found on the downstream flange of a horizontal girder on a tainter gate. The crack is an edge crack similar to that shown in Figure 6-10. Prior to the inspection, no indication of damage had been reported. Since the cracked girder is a main framing element of the tainter gate, an immediate assessment of its critical nature is required. The crack is near the midlength of the girder. The girder flange is 35.6 cm (14 in.) wide and 3.8 cm (1.5 in.) thick.

(2) To evaluate this crack, a fracture analysis must be conducted. For this example, a linear-elastic fracture mechanics (LEFM) analysis will be used. The first step in performing the analysis is to obtain data on the three key parameters necessary for any fracture analysis: the crack size and geometry, the nominal stress in the member or component σ, and the critical stress intensity factor, K_{Ic} or K_c.

(3) The crack size and the geometry have already been determined from the inspection. For an LEFM analysis, the nominal member stress is required. For this case, the nominal girder flange stress can be determined from a plane frame analysis similar to that used in the design of tainter gate girders. An analysis showed that the nominal girder flange stress in the vicinity of the crack was 117.2 MPa (17 ksi) in tension.

(4) The next step in the analysis is to determine the fracture toughness. A review of the hypothetical design documents indicated that the gate had been fabricated from A36 steel. Since K_{Ic} testing (ASTM E399) of mild steels at reasonable service temperatures is impractical if not impossible, the fracture toughness will be determined from correlations with CVN data. As a first estimate, published CVN data for A36 steel will be used. This can be only an estimate, since K_{Ic} values can vary significantly for the same type of steel. K_{Ic} is also very dependent on temperature, so a minimum operating temperature for the structure must be established. Based on A36 steel CVN data (Barsom and Rolfe 1987), Figure 7-4 shows the approximation of K_{Ic} as a function of temperature. The curve on the left is calculated from the two-stage CVN-K_{Id}-K_{Ic} correlation (valid for the lower shelf and the lower end of the transition region; see paragraph 7-1*b*), and the curve on the right is from the upper shelf CVN-K_{Ic} correlation (Equation 7-3). The heavy line of each curve indicates the range in which the correlations are valid, as discussed in paragraph 7-1. The minimum service temperature for this example is -31.6 °C (-25 °F). Since neither curve is valid at this temperature, an estimate for K_{Ic} is determined by linear interpolation between the two correlations as indicated by the dashed line in Figure 7-4. This interpolation indicates that K_{Ic} is approximately 62.6 Mpa-$\sqrt{\text{m}}$ (57 ksi-$\sqrt{\text{in.}}$) at -31.6 °C (-25 °F). Conservatively, an estimate of K_{Ic} of 55 MPa-$\sqrt{\text{m}}$ (50 ksi-$\sqrt{\text{in.}}$) is selected for use in the analysis.

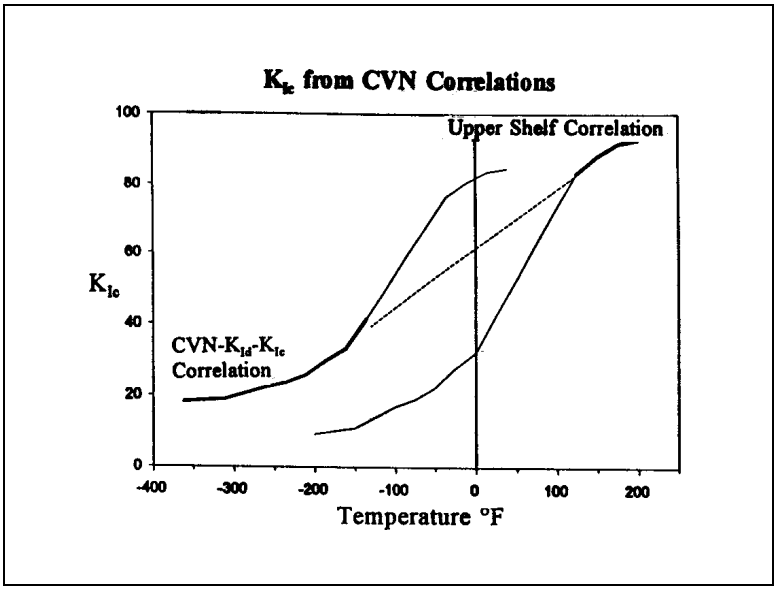

Figure 7-4. CVN-K_{Ic} correlations (°C = 5/9 (°F – 32); 1 ksi-$\sqrt{in.}$ = 1.099 MPa-$\sqrt{m}$)

(5) Since the crack size and geometry of detail are known and the stress level and material fracture toughness have been estimated, the crack can be evaluated for fracture by calculating the stress intensity factor and comparing to the fracture toughness. For a single-edge crack perpendicular to the stress field in a finite-width plate, the stress intensity factor incorporating a factor of safety (FS), K_{If}, is given by

$$K_{If} = 1.12\sigma\sqrt{\pi\, a\, FS} \bullet k\left(\frac{a\ FS}{b}\right) \tag{7-7}$$

where

a = crack size

k = function of a and b

b = half-width of the plate

(Tabulated values for k and stress intensity factor formulas for other crack geometries are given in Chapter 6.) For a factored crack length-to-plate half-width ratio of $(a \times FS)/b = (3.5 \times 2)/7 = 1.0$, $k = 2.55$, then

$$K_{If} = 1.12\,(117.2)\sqrt{\pi\ \ (0.09)\,(2)} \bullet 2.55 = 250\ \text{MPa-}\sqrt{\text{m}} = 288\ \text{ksi-}\sqrt{\text{in.}} \tag{7-8}$$

Since K_{If} is greater than $K_{Ic} = 54.95$ MPa-$\sqrt{m}$ (50 ksi-$\sqrt{in.}$), an unsafe condition exists for plane-strain conditions. Checking the plane strain assumption with Irwin's β factor from Equation 2-2:

$$\beta_{Ic} = \frac{1}{0.038}\left(\frac{55}{248}\right)^2 = 1.3 > 0.4 \tag{7-9}$$

Since $\beta_{Ic} > 0.4$, the plane-strain condition assumption is not valid and the fracture toughness is represented by the critical stress intensity factor K_c. Using Equation 7-6 to estimate K_c (even though there is considerable deviation from plane strain condition) gives

$$K_c^2 = K_{Ic}^2 \left(1 + 1.4\ \beta_{Ic}^2\right) = 55^2 \left(1 + 1.4 \cdot 1.29^2\right) = 10{,}072\ \left(\text{MPa-}\sqrt{\text{m}}\ \right)^2 \left[8{,}324 \left(\text{ksi-}\sqrt{\text{in.}}\ \right)^2\right]$$

$$K_c = 100\ \text{MPa-}\sqrt{\text{m}}\ \left(91\ \text{ksi-}\sqrt{\text{in.}}\ \right) \qquad (7\text{-}10)$$

$$K_c < K_{If} = 250\ \text{MPa-}\sqrt{\text{m}}\ \left(228\ \text{ksi-}\sqrt{\text{in.}}\ \right)$$

(6) Since K_c is less than K_{If}, an unsafe condition exists. This indicates that an immediate repair plan should be developed and implemented. If the repair will be costly and/or substantially affect the function of the project, a more accurate analysis should be made. The analysis was based on an estimation of K_{Ic} that may not accurately reflect the plane-strain fracture toughness of the material, and the approximation of K_c from K_{Ic} introduces more uncertainty in the estimation of the fracture toughness of the girder flange. A more exact analysis would require having tests conducted on the girder material so that a more accurate value of K_c may be obtained. A CTOD test, which can be used to estimate K_c (Equation 7-5), would likely be most appropriate because of the uncertainty in correlating CVN data at the service temperature. Alternatively, an elastic-plastic fracture assessment can be performed as outlined in Chapter 6.

d. Lock gate fracture example. Cracks of various shapes were revealed on two tension members on a lock gate by nondestructive testing inspection. One member has the cross-sectional dimensions of 10 cm (4 in.) thick by 30.5 cm (12 in.) wide. The other member is 2.5 cm (1 in.) thick by 30.5 cm (12 in.) wide. The crack types and shapes include single-edge crack; through-thickness center crack; surface crack along the 0.3-m (12-in.) side ($a/2c$ = 0.1 and 0.2), and embedded circular cracks. The material properties at the minimum service temperature of –1.1 °C (30 °F) were determined by material testing and are summarized as follows:

σ_{ys} = offset yield strength of 345 MPa (50 ksi)

σ_{ult} = 552 MPa (80 ksi)

E = 206,840 MPa (30,000 ksi)

K_{Ic} = 66 MPa-$\sqrt{\text{m}}$ (60 ksi-$\sqrt{\text{in.}}$)

K_{Id} = 44 MPa-$\sqrt{\text{m}}$ (40 ksi-$\sqrt{\text{in.}}$)

δ_{crit} = critical CTOD value of 0.0052 cm (0.002 in.) (static)

δ_{crit} = 0.0025 cm (0.001 in.) (dynamic)

From structural analysis, the maximum applied tensile stress is 207 MPa (30 ksi). For each cracked member, the critical crack size will be determined for each cracking condition under static loading and dynamic loading, respectively:

(1) Example for 10-cm (4-in.) by 30-cm (12-in.) plate:

$$\beta_{Ic} = \frac{1}{t}\left(\frac{K_{Ic}}{\sigma_{ys}}\right)^2 = \frac{1}{10}\left(\frac{66}{345}\right)^2 = 0.36$$

$\beta_{Ic} < 0.4$; therefore, LEFM is applicable.

(a) Single-edge crack (see Figure 6-10):

$$K_I = 1.12\sigma\sqrt{\pi a}\ k\left(\frac{a}{b}\right)$$

where σ is the nominal stress.

$$C = 1.12\ \sqrt{\pi}\ k\left(\frac{a}{b}\right) \text{ in Equation 6-1}$$

Assume $k(a/b) = 1.0$. The critical discontinuity size is calculated as

$$a_{cr} = \frac{1}{\pi}\left(\frac{K_{Ic}}{1.12\sigma}\right)^2 = 2.59 \text{ cm } (1.02 \text{ in.}) \text{ (Equation 6-2 with no factor of safety)}$$

(a/b) = 0.17 and $k(a/b)$ = 1.06; therefore, iteration is needed for a_{cr} and $k(a/b)$. After iteration, a_{cr} = 2.34 cm (0.92 in.) ($k(a/b)$ = 1.05). With FS = 2.0, a_{cr} = 0.5 (2.34) = 1.17 cm (0.46 in.) for dynamic loading:

$$a_{cr} = \frac{0.5}{\pi}\left(\frac{K_{Id}}{1.12\sigma}\right)^2 = 0.58 \text{ cm } (0.23 \text{ in.})$$

(b) Through-thickness center crack (Figure 6-8). Calculate the stress intensity factor:

$$K_I = \sigma\ \sqrt{\pi a}\ \sqrt{\frac{2b}{\pi a}\ \tan\left(\frac{\pi a}{2b}\right)}$$

Assume

$$\sqrt{\frac{2b}{\pi a}\ \tan\left(\frac{\pi a}{2b}\right)} = 1.0$$

$$a_{cr} = \frac{1}{\pi}\left(\frac{K_{Ic}}{\sigma}\right)^2 = 3.23 \text{ cm } (1.27 \text{ in.})$$

$$\sqrt{\frac{2b}{\pi a}\ \tan\left(\frac{\pi a}{2b}\right)} = 1.02$$

After iteration, a_{cr} = 3.1 cm (1.22 in.). With FS = 2.0, a_{cr} = 3.1/2 = 1.55 cm (0.61 in.) and for dynamic loading,

$$a_{cr} = \frac{0.5}{\pi}\left(\frac{K_{Id}}{\sigma}\right)^2 = 0.71 \text{ cm } (0.28 \text{ in.})$$

(c) Surface crack along the 30.5-cm (12-in.) side ($2c$ is the length of the surface crack along the slope of the component; see Figure 6-15):

- $a/2c = 0.1$

$$K_I = 1.12\ \sigma\ \sqrt{\pi \frac{a}{Q}}\ \ M_K$$

$$\frac{\sigma}{\sigma_{ys}} = \frac{207}{345} = 0.6$$

where Q is the flow shape parameter defined by Figure 6-14 and M_k is a variable that describes the effect of a/t on K_I.

From Figure 6-14, $Q = 1.02$, assume $M_k = 1.0$

$$a_{cr} = \frac{Q}{\pi}\left(\frac{K_{Ic}}{1.12\,\sigma}\right)^2 = 2.64 \text{ cm (1.04 in.)}\ \ (a/t = 0.26;\ M_k = 1.0)$$

With $FS = 2.0$, $a_{cr} = 2.64/2 = 1.32$ cm (0.52 in.), and for dynamic loading,

$$a_{cr} = \frac{0.5\ Q}{\pi}\left(\frac{K_{Ic}}{1.12\,\sigma}\right)^2 = 0.58 \text{ cm (0.23 in.)}$$

- $a/2c = 0.2$

From Figure 6-14, $Q = 1.24$, assume $M_k = 1.0$

$$a_{cr} = \frac{Q}{\pi}\left(\frac{K_{Ic}}{1.12\,\sigma}\right)^2 = 3.2 \text{ cm}\ \ (1.23 \text{ in.})\ \ (a/t = 0.32;\ M_k = 1.0)$$

With $FS = 2.0$, $a_{cr} = 3.2/2 = 1.6$ cm (0.63 in.), and for dynamic loading,

$$a_{cr} = \frac{0.5\,Q}{\pi}\left(\frac{K_{Ic}}{1.12\,\sigma}\right)^2 = 0.71 \text{ cm (0.28 in.)}$$

(d) Embedded circular crack (see Figure 6-14).

$$K_I = \sigma\ \sqrt{\pi \frac{a}{Q}}$$

$a/2c = 0.5$; from Figure 6-14, $Q = 2.4$

with $FS = 2.0$,

$$a_{cr} = \frac{0.5\,Q}{\pi}\left(\frac{K_{Ic}}{\sigma}\right)^2 = 3.89 \text{ cm (1.53 in.)}$$

and for dynamic loading:

$$a_{cr} = \frac{0.5\,Q}{\pi}\left(\frac{K_{Ic}}{\sigma}\right)^2 = 1.73 \text{ cm (0.68 in.).}$$

(2) Example for 2.5-cm (1-in.) by 30-cm (12-in.) plate:

$$\beta_{Ic} = \frac{1}{t}\left(\frac{K_{Ic}}{\sigma_{ys}}\right)^2 = \frac{1}{0.025}\left(\frac{66}{345}\right)^2 = 1.46.$$

$\beta_{Ic} > 0.4$; therefore, elastic-plastic fracture mechanics is applicable.

Determine the allowable discontinuity parameter $\bar{a}_m$ (paragraph 6-5*b*).

$$\bar{a}_m = C\left[\frac{\delta_{crit}}{\varepsilon_y}\right] \quad \text{(Equation 6-4)}$$

where ε_y is the yield strain of the material

$$\varepsilon_y = \frac{\sigma_{ys}}{E} = \frac{345}{206{,}843} = 0.0017$$

$$\frac{\sigma}{\sigma_{ys}} = \frac{207}{345} = 0.6$$

From Figure 6-20, $C = 0.44$

For static loading

$$\bar{a}_m = 0.44\left(\frac{0.0052}{0.0017}\right) = 1.32 \text{ cm (0.52 in.)}$$

For dynamic loading

$$\bar{a}_m = 0.44\left(\frac{0.0025}{0.0017}\right) = 0.65 \text{ cm (0.26 in.)}$$

Critical crack lengths can be determined for various crack shapes from the allowable discontinuity parameter $\bar{a}_m$ (paragraph 6-5*b*).

7-3. Example Fatigue Analysis

This example shows how to apply fatigue analysis to determine expected life given an initial flaw size a_i. For this case, consider an initial surface flaw of the type shown in Figure 6-15 with $a/2c = 0.25$. The member is a 10-cm- (4-in.-) thick plate of ASTM A572/572M Grade 345 (50) steel. The critical stress intensity factor (fracture toughness) K_{Ic} of this steel is 66 MPa-$\sqrt{\text{m}}$ (60 ksi-$\sqrt{\text{in.}}$) at the minimum service temperature.

a. The maximum stress level is 207 MPa (30 ksi) and the minimum stress is zero. A curve relating the initial surface flaw size a_i to number of cycles to failure N_p will be developed. From Figure 6-15

$$K_I = 1.12\,\sigma\sqrt{\pi\frac{a}{Q}}\;M_K$$

$\frac{\sigma}{\sigma_{ys}} = \frac{207}{345} = 0.6$ and $Q = 1.39$ (Figure 6-14).

Assume $M_k = 1.0$.

With $FS = 2.0$,

$$a_{cr} = \frac{0.5Q}{\pi}\left(\frac{K_{Ic}}{1.12\,\sigma}\right)^2 = 1.8 \text{ cm (0.71 in.)}$$

(for crack sizes up to $a = 1.8$ cm (0.71 in.), $M_k = 1.0$) and for ferrite-pearlite steel, $da/dN = 6.9\times10^{-9}\,(\Delta K_I)^3$ (Equation 6-8):

$$\Delta K_I = 1.12\Delta\sigma\sqrt{\pi\frac{a}{Q}} = 348.5\sqrt{a}\quad \text{MPa}\sqrt{\text{m}}\quad \left(50.5\sqrt{a}\quad \text{ksi}\sqrt{\text{in.}}\right)$$

b. Fatigue life can be determined as:

$$N = \int_{a_i}^{a_{cr}} \frac{da}{(6.9\times10^{-9})(\Delta K_I)^3}$$

$$N = \frac{1}{(6.9\times10^{-9})(348.5)^3}\int_{a_i}^{a_{cr}} a^{-3/2}\,da$$

$$N = (6.9)\left(\frac{1}{\sqrt{a_i}} - \frac{1}{\sqrt{a_{cr}}}\right)$$

c. The curve for fatigue life N as a function of initial crack length a_i for this example is shown in Figure 7-5.

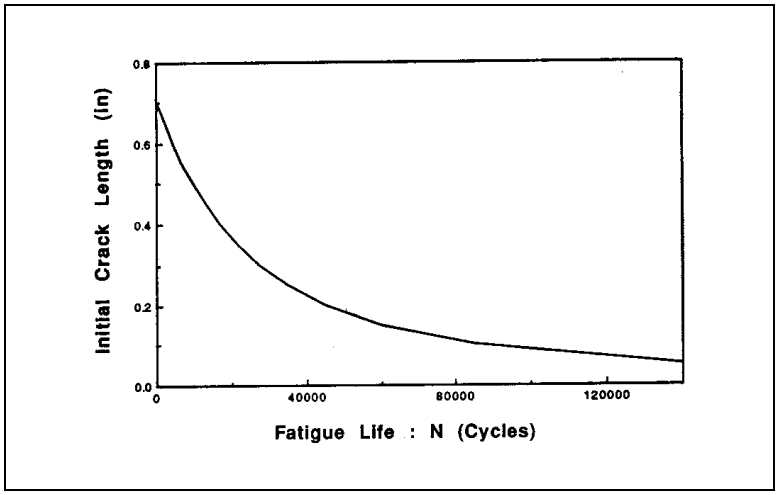

Figure 7-5. Fatigue life *N* versus initial crack-length a_i curve (1 in. = 2.4 cm)

7-4. Example of Fracture and Fatigue Evaluation

a. Single-edge crack.

(1) Figure 7-6 shows a horizontal girder with a single-edge crack. The initial crack length is assumed to be 3 mm (1/8 in.). The flange plate containing the edge crack is assumed to be under a cyclic load from zero to maximum tension (i.e., fatigue ratio $R = 0$). The stress ranges vary from 124 MPa (18 ksi) to 186 MPa (27 ksi). The fatigue life can be calculated using the following crack growth equation (Equation 6-8):

$$\frac{da}{dN} = 6.9 \times 10^{-9} \ (\Delta K_I)^3$$

where

$$K_I = 1.12 \ \sigma \ \sqrt{\pi a} \ \ k\,(a/b)$$

By integrating the crack growth equation, the life of the propagating crack can be determined for any crack length:

$$N = \int_{a_i}^{a_{cr}} \frac{da}{(6.9 \text{ x } 10^{-9})\,(\Delta K_I)^3}$$

where K_I is a function of crack length

and from Equation 6-2:

$$a_{cr} = \frac{1}{\pi}\left(\frac{K_{Ic}}{1.12\,\sigma\,k\left(\frac{a}{b}\right)}\right)^2$$

With K_{Ic} assumed to be 38.4 MPa-$\sqrt{\text{m}}$ (35 ksi-$\sqrt{\text{in.}}$) and a maximum stress of 124 MPa (18 ksi), $a_{cr} = 2.3$ cm (0.89 in.) using the procedure described in paragraph 7-2*d*(1)(a).

(2) Figure 7-7a shows the calculated crack growth versus life cycle for a stress range of 124 MPa (18 ksi) (1/2 σ_{ys}). The remaining life *N*, calculated by the equation for the life of the propagating crack in (1) above, is 207,700 cycles. If the structure operates 10,000 times per year, then the remaining life of the girder is:

$$\frac{207{,}700}{10{,}000} = 20.8 \text{ years}$$

Critical crack length (determined by Equation 6-2) is a function of external loading as shown in Figure 7-7b. Figure 7-7c shows the fatigue life for stress ranges varying from 124 MPa (18 ksi) to 186 MPa (27 ksi) calculated using the crack growth equation with variable stress and a_{cr}. The remaining life of the girder flange containing a 3-mm (1/8-in.) initial crack is shown in the figure as a function of stress.

b. Double-edge crack. A girder flange containing double-edge cracks is shown in Figure 7-8. The crack growth curves were calculated for stress ranges varying from 69 to 138 MPa (10 to 20 ksi). The same integration procedure as used for the single-edge crack case is employed for calculating the fatigue life. A 3-mm

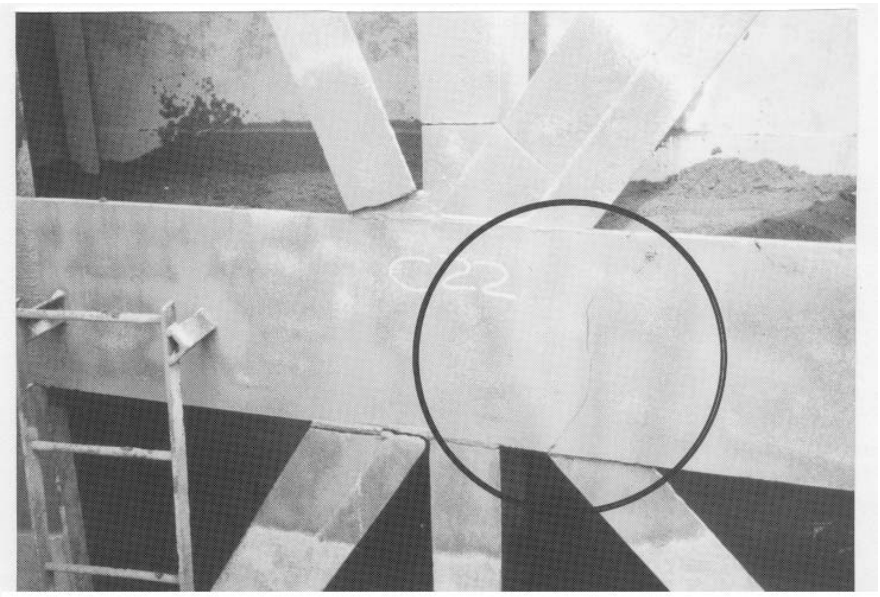

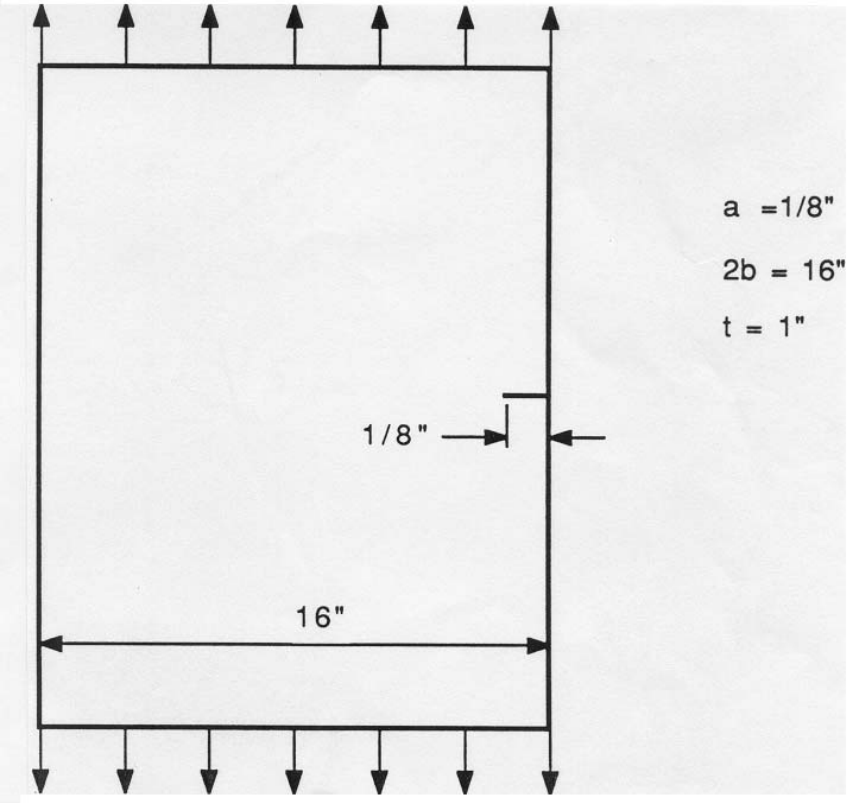

Figure 7-6. A single-edge cracked girder (1 in. = 2.54 cm)

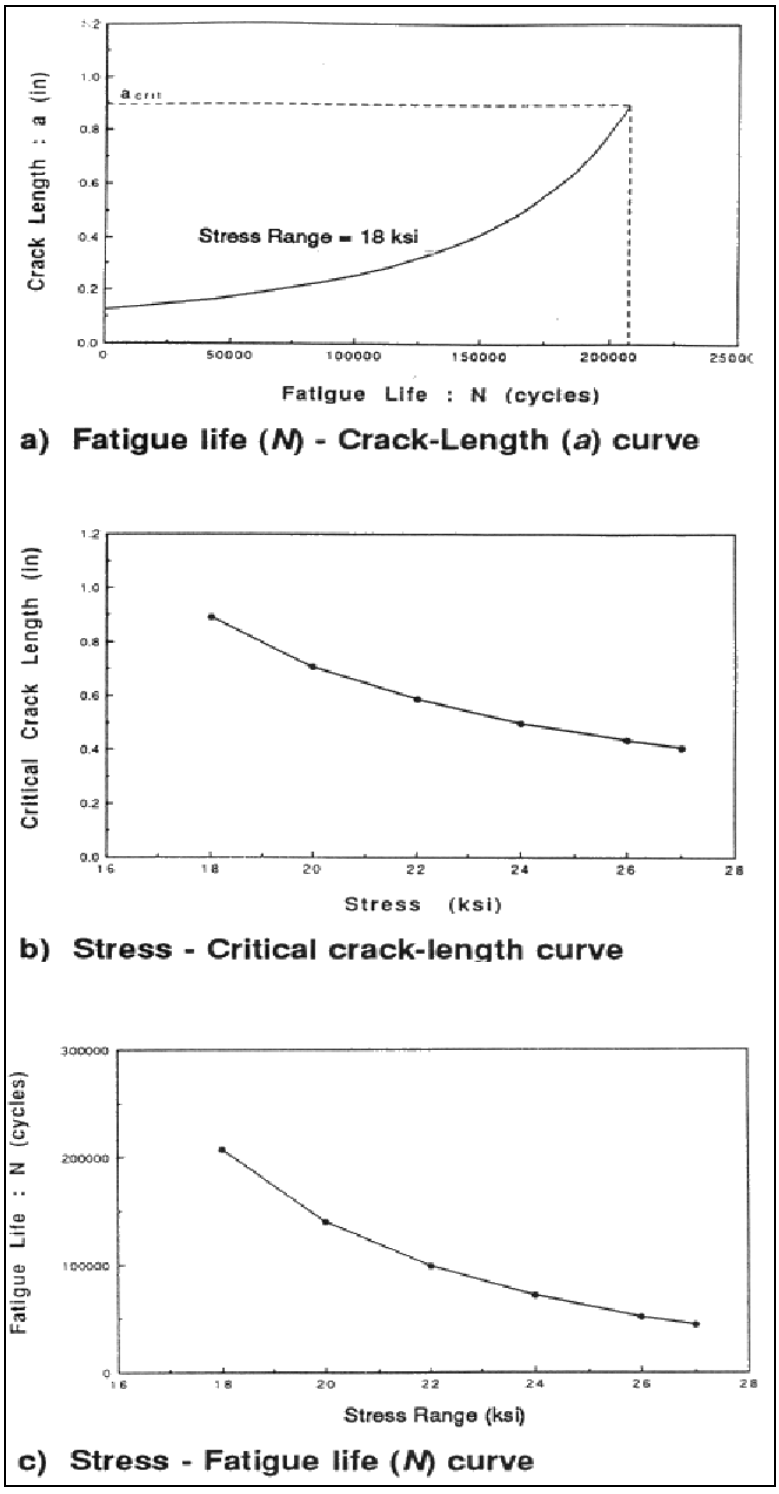

Figure 7-7. Curves for fatigue life of a flange with a single-edge crack (1 in. = 2.54 cm; 1 ksi = 6.89 MPa)

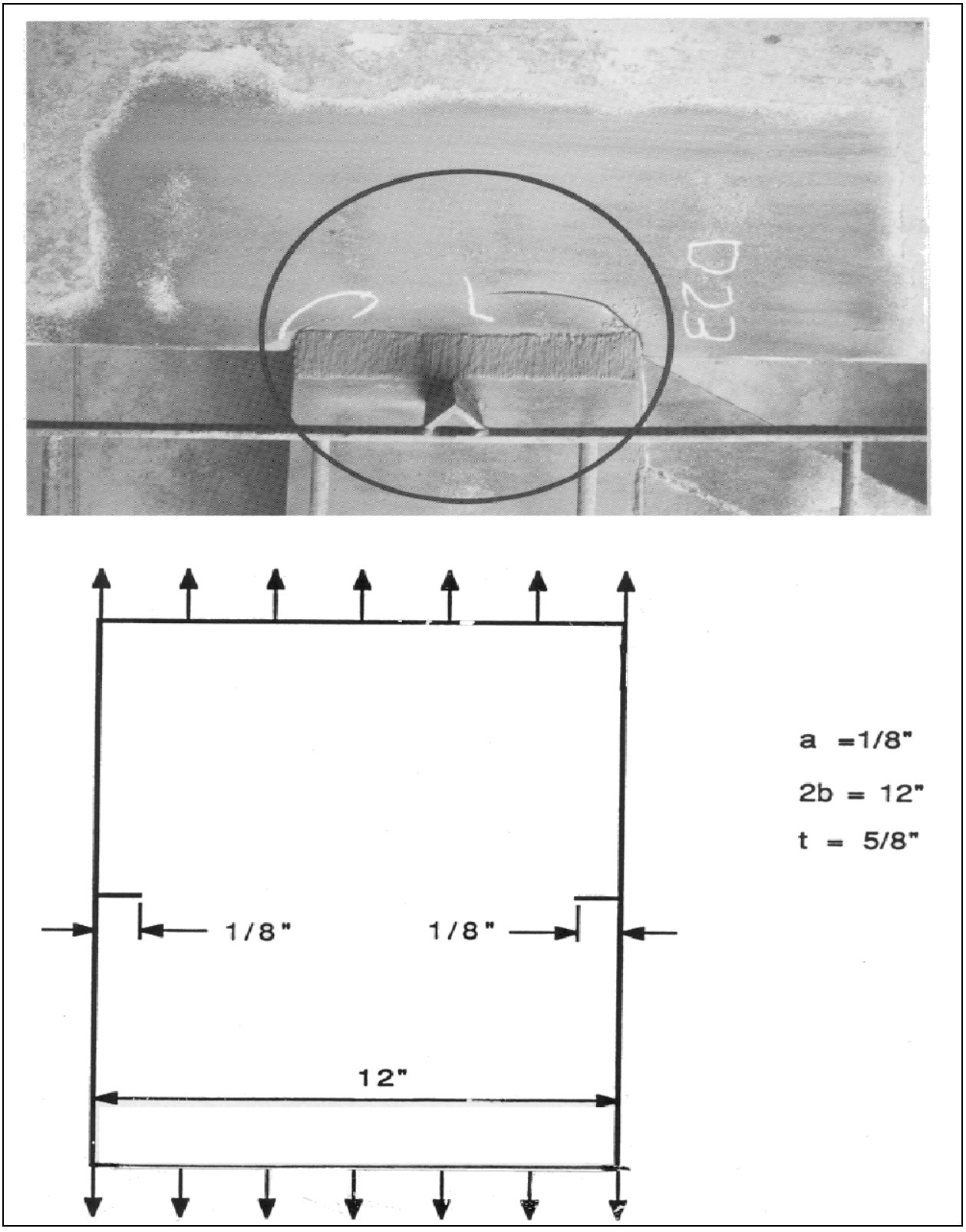

Figure 7-8. A double-edge cracked flange (1 in. = 2.54 cm)

(1/8-in.) initial crack length is also assumed in this case. The predicted crack growth curve for stress range of 124 MPa (18 ksi) is shown in Figure 7-9a. Figure 7-9b shows the relationship between stress and critical crack length. The remaining life of the girder flange plate for various stress ranges is also shown in Figure 7-9c.

c. Surface crack. Figure 7-10 shows a crack assumed to have initiated in the diagonal bracing member from a surface crack at the corner of the bracket. It is assumed that the crack propagated through the thickness of the bracing member and then grew toward the edge of the flange plate. A single-edge crack condition similar to the first example case was developed. The fracture and fatigue analysis of this example consists of three propagation steps.

(1) The first step is to analyze the crack propagation of a hemispheric surface crack having an initial radius of 1.6 mm (1/16 in.). When the surface crack breaks through the surface on the other side of the plate (i.e., the radius of hemispheric crack becomes the same as the plate thickness of 9.5 mm (3/8 in.)), a through-thickness crack condition is reached.

(2) The second step is to analyze crack growth of a plate containing a through-thickness crack. Once the through-thickness crack reaches the edge of the plate, the single-edge crack condition is developed.

(3) The third step is to analyze crack growth of the edge crack. The total remaining life of the diagonal bracing member from the initial hemispheric surface crack can be determined by adding the three propagation lives. The calculated crack growth curve for a stress range of 124 MPa (18 ksi) is shown in Figure 7-11a. The total remaining life and critical crack length are also shown in Figure 7-11b and c for stress ranges varying from 69 to 138 MPa (10 to 20 ksi).

d. Inspection schedule. The inspection schedule can be determined from the fatigue life curve of the single-edge crack in the primary member. The maximum stress range is assumed as 124 MPa (18 ksi). The procedure is shown in the following steps.

(1) Determine critical crack length:

a_{cr} = 2.26 cm (0.89 in.) (paragraph 7-4*a*)

(2) Determine crack length when repair is needed (Figure 6-23):

a_r = 2.26/2 = 1.13 cm (0.45 in.) (FS = 2.0)

(3) Determine fatigue life from fatigue life N versus crack length a curve:

N = 160,000 cycles; 160,000/10,000 = 16 years (10,000 cycles/year)

Therefore, the girder should be inspected within 16 years after the initial crack (a_i = 3 mm (1/8 in.)) was found.

7-5. Structural Steels Used on Older Hydraulic Steel Structures

Steel standards for the period when many hydraulic steel structures were constructed are of interest from both a structural evaluation and a repair and maintenance standpoint. In a structural evaluation, the characteristics of corrosion resistance, fracture resistance, crack propagation rate, and stability of properties with seasonal temperature changes are considered important parameters. The weldability of steels is also of interest since welding will likely be considered for repair and maintenance procedures even for riveted structures. However, at the time the gates were constructed, these properties probably were not determined or even much considered.

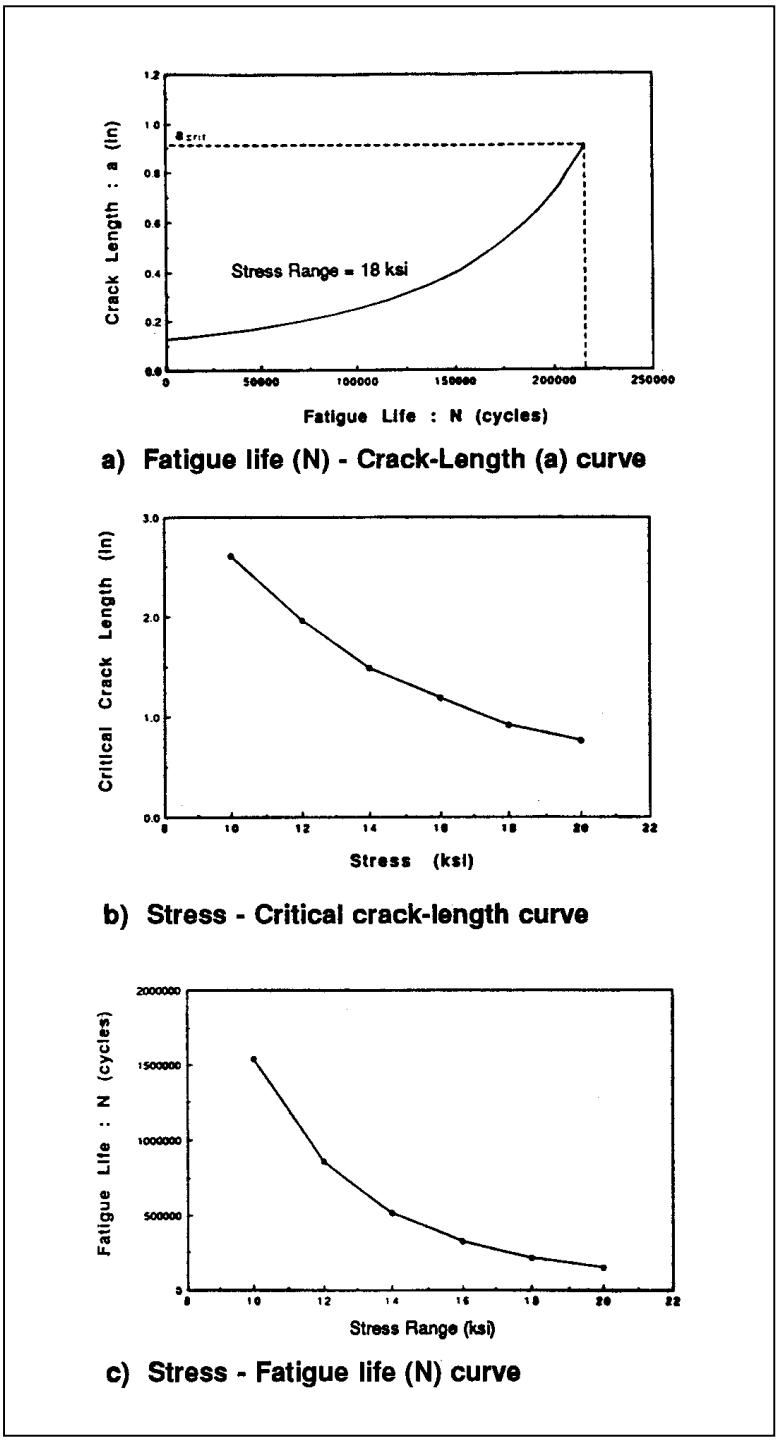

Figure 7-9. Curves for fatigue life of a flange with a double-edge crack (1 in. = 2.54 cm; 1 ksi = 6.89 MPa)

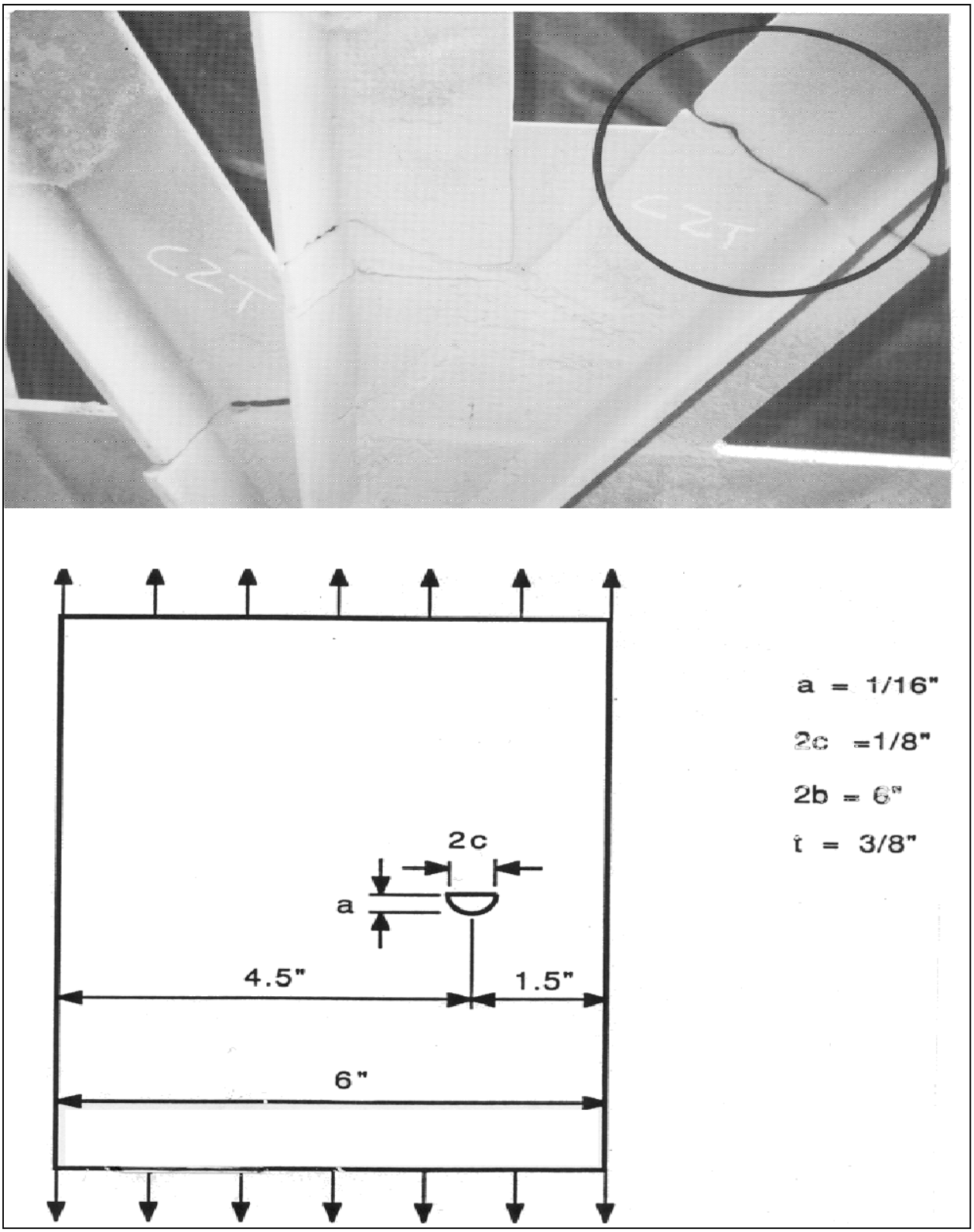

Figure 7-10. A stiffening member with a crack (1 in. = 2.54 cm)

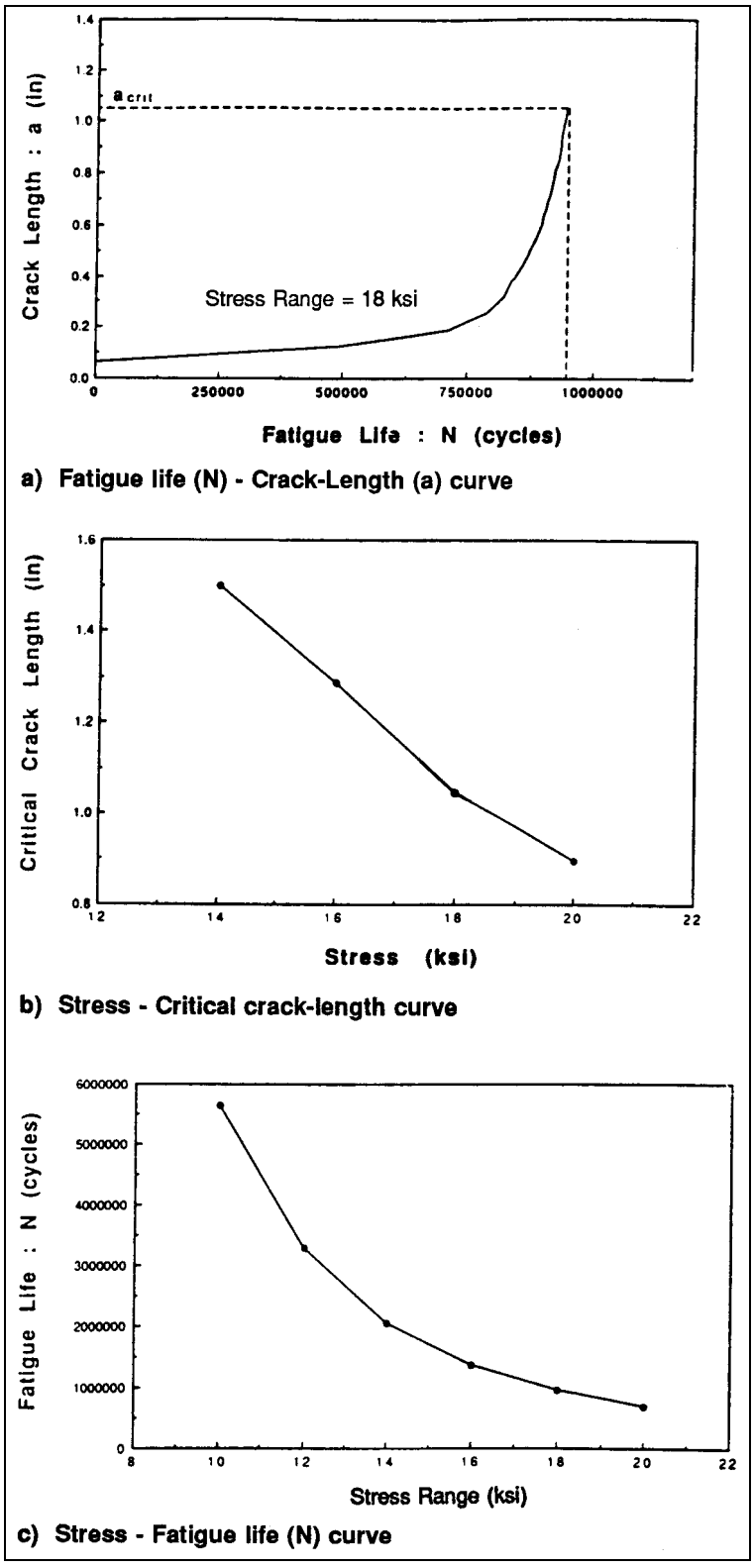

Figure 7-11. Curves for fatigue life of a stiffening member with a surface crack (1 in. = 2.54 cm; 1 ksi = 6.89 MPa)

a. Structural steel standards.

(1) In the 1930's when many hydraulic steel structures were designed and built, several structural steels were commonly in use. In the mid-1930's, structural steel could have been either ASTM A7-33T or ASTM A9-33T steel (Ferris 1953). A7 steel was generally regarded at the time as a steel for bridges, whereas A9 steel was a steel for buildings. The primary differences between the two were that A7 steel had a lower maximum allowable phosphorus content and had a limit on sulfur content compared with A9 steel. A7 steel also was restricted to open-hearth or electric-furnace production and excluded the older acid-bessemer production. These compositional and production restrictions suggest that A7 bridge steel was recognized as the premium steel of the two. For a brief period (1932-33), structural steel also could have been supplied as ASTM A140 steel, which was a tentative replacement for both A7 and A9 steels (Ferris 1953).

(2) Steel identified as silicon steel on design drawings is mostly likely ASTM A94-25T structural silicon steel. This was a high-strength steel with a specified minimum silicon content that attained its high strength (minimum yield point of 310 MPa (45 ksi) and tensile strength of 552 to 655 MPa (80 to 95 ksi)) through a high level of carbon (0.44 percent maximum). It also had limits on its phosphorus and sulfur contents.

(3) An important characteristic of the early steels, regardless of whether they were A7, A9, A140, or A94 silicon steel, is that they had either no specified level or a high level of carbon in their composition. Consequently, the carbon level was either not rigorously controlled or was moderately high, with the result that the steels probably had and have only poor to fair weldability. The specification for A94 structural silicon steel specifically limits welding and specifies a preheat condition when welding must be done. Of course, the steels were being used for riveted structures, so weldability was not then a concern to designers. But it needs to be considered for weld repairs or maintenance contemplated today.

(4) In 1939, A7 and A9 were consolidated into a single specification, A7 steel (ASTM A7-39) for bridges and buildings, which then became the single specification for structural steel. In 1954 a new structural steel for welding, A373 steel, was introduced (ASTM A373-58T). Both A7 and A373 steels were consolidated in 1965 into one specification, A36 steel (ASTM A36-60T), which is the basic structural steel today and is used for both welded and bolted applications.

b. Rivet steel standards.

(1) Rivet steel was not typically specified by steel grade, but only as structural steel, carbon steel, or as rivets. However, the allowable shear stress for power-driven rivets was occasionally identified as 82.7 MPa (12 ksi), and the allowable bearing stress as 165.4 MPa (24 ksi). Until 1932, rivet steel was included in the ASTM A7 and A9 specifications, but with lower yield and tensile strengths than structural steel (Ferris 1953). However, in 1932, ASTM A141 was issued as a tentative specification for structural rivet steel, with somewhat more enhanced strength requirements than earlier. More restrictive diameter tolerances were included in a 1936 tentative revision. Until 1949, rivet yield strength was specified as one-half times the tensile strength or not less than 193 MPa (28 ksi). In 1949, the yield strength for A141 rivet steel was changed to 193 MPa (28 ksi) minimum (Ferris 1953). In 1960, A141 rivet steel was incorporated into the new tentative A36 steel specification (ASTM A36-60T).

(2) In 1936, a new tentative specification, ASTM A195, was issued for high-strength structural rivet steel, for rivets produced from structural silicon steel (ASTM A195-36T). As opposed to A141 rivet steel, A195 rivet steel had carbon, manganese, silicon, and copper requirements. In addition, A195 rivet steel yield strength was specified as one-half times the tensile strength or not less than 262 MPa (38 ksi). A195 steel rivets were to be used with A94 structural silicon steel, although the use of A141 steel rivets may have continued.

(3) In 1964, a new specification, ASTM A502, was published for steel structural rivets, and superseded ASTM A141 and A195. The later version of this specification (ASTM A502) covers three grades of steel rivets: general-purpose carbon steel rivets, carbon-manganese steel rivets for use with high-strength carbon and high-strength low-alloy steels, and rivets comparable to ASTM A588 weathering steel. The later specification includes hardness requirements but not tensile and yield strength requirements.

c. Allowable and yield stresses. During the same period that A7 steel was evolving, the American Institute of Steel Construction (AISC) changed their basic allowable working stress for structural steel only once, raising it in 1936 from 124 to 138 MPa (18 to 20 ksi) (Ferris 1953). The ASTM requirement for minimum yield point during this period was generally one-half times the tensile strength, or not less than 207 MPa (30 ksi); in 1933, the minimum of 207 MPa (30 ksi) was raised to 227.5 MPa (33 ksi) for plate and shape products. When A373 steel was introduced, that steel had a minimum yield point of 220.6 MPa (32 ksi), suggesting that to improve weldability at that time, some sacrifice in strength was necessary. Only when A36 steel was introduced in 1960 in a tentative specification (ASTM A36-60T) did the minimum yield point for structural steel plates and shapes increase to 248 MPa (36 ksi). By that time, weldability and welding practices for structural steel had markedly improved and standardized.

d. Weldability of earlier steels.

(1) A very good reference that discusses the weldability of steels, including steels that have limited weldability, is the monograph "Weldability of Steels" published by the Welding Research Council (Stout et al. 1987). Now in its fourth edition, the monograph has chapters on the properties of steel related to weldability, factors affecting weldability in fabrication, and the weldability of different steels.

(2) For early steels, reference can be made to the first edition of the monograph (Stout and Doty 1953) which includes suggested (as of 1953) welding practices for A7 steel meeting the tentative specification ASTM A7-50T. However, even the first edition does not include data for A9 or A94 steels. A copy of the suggested (1953) practices for A7 steel is listed in Table 7-1. For thicknesses up to 1 in. (the normal case for hydraulic steel structures), a comparison of the recommended practices in Table 7-1 suggests that for carbon levels of 0.25 percent or less, no special welding requirements are needed for A7 steel. However, as the carbon level increases, more stringent practices are needed. Because A7 steel did not have a specified carbon level, repair and maintenance welding should be conducted favoring the more stringent practices. For other early steels or for steels of unknown specification, ANSI/AWS D1.1 provides optional methods for determining welding requirements based on the chemical composition of the steel.

(3) A generally conservative practice for repair and maintenance welding on riveted spillway gates is to use the practices for A7 steel in Table 7-1, with the assumption that the carbon level is between 0.26 and 0.30 percent.

Table 7-1
Suggested Practices for Sound Welding with A7 Steel (After Stout and Doty 1953)

A7 Steel

CONDITIONS REQUIRING NO PREHEATING, POSTHEATING, OR SPECIAL ELECTRODES

Steel Specification	Conditions for Which No Special Precautions Are Required		Remarks	Grade or Quality	Specification Requirements (Abridged)									
					Composition								Tensile Properties	
	Carbon Range, %	Thickness Range, in.			C	Mn	Si	Ni	Cr	Mo	Other	Yield Point psi	Tensile Strength psi	Elongation %
ASTM A7-50T Steel for bridges and buildings	Up to 0.25, incl.	Up to 1, incl.	Over 1 in., see Table II	...	(Not specified)	(Not specified)	(Not specified)	...	...	...	0.20 min. Cu when specified	33,000 min.	60,000-72,000	21 in 8 inches (min.)
	0.26 - 0.30, incl.	Up to 1/2, incl	Over 1/2 in., see Table II											
			Over 0.30 carbon see Table II											

TABLE II. CONDITIONS REQUIRING SOME CONTROL OVER HEAT INPUT AND REQUIRING LOW HYDROGEN ELECTRODES OR PREHEAT AND GENERALLY POSTHEATING

Conditions for Which Precautions Are Required			
Carbon Range %	Thickness Range in.	Recommended Arc Welding Conditions General Notes: Electrodes should be of suitable composition when alloy steels are welded. Welding conditions are not given for materials over 4 inches thick.	
Up to 0.25 incl.	Over 1-2, incl.	Condition A or B	Condition A = 100°F minimum preheat and interpass temperature, 1100-1250°F stress relief optional. Condition B = No welding below 10°F, EXX15 or EXX16 electrode, 1100-1250°F stress relief optional. Condition C = 200°F minimum preheat and interpass temperature, 1100-1250°F stress relief optional.
	Over 2-4, incl.	Condition C	
0.26-0.30 incl.	Over 1/2-1, incl.	Condition A or B	
	Over 1-2, incl.	Condition B or C	
	Over 2-4, incl.	See Table III	
0.31-0.35 incl.	Up to 1/2, incl.	Condition A or B	
	Over 1/2-1, incl.	Condition B or C	
	Over 1-4, incl.	See Table III	

TABLE III. CONDITIONS REQUIRING PREHEAT, SPECIAL WELDING TECHNIQUES, AND POSTHEATING AND/OR PEENING

Conditions for Which Precautions Are Required			
Carbon Range %	Thickness Range in.	Recommended Arc Welding Conditions General Notes: Electrodes should be of suitable composition when alloy steels are welded. Welding conditions are not given for materials over 4 inches thick.	
0.26-0.30 incl.	Over 2-4, incl.	Condition J	Condition J = 100°F minimum preheat and interpass temperature with EXX15 or EXX16 electrode or 300°F preheat with other than EXX16 electrode, 1100-1250°F stress relief optional, peening may be necessary for thicknesses over 1 inch. Condition K = 200°F minimum preheat and interpass temperature with EXX15 or EXX16 electrode or 300°F preheat with other than EXX15 or EXX16, 1100-1250°F stress relief optional, peening may be necessary for thicknesses over 1 inch.
0.31-0.35 incl.	Over 1-2, incl.	Condition J	
	Over 2-4, incl	Condition K	